

Extreme Optical Properties Tuned Through Phase Substitution in a Structurally Optimized Biological Photonic Polycrystal

Xia Wu, Andreas Erbe, Dierk Raabe, and Helge-Otto Fabritius*

Biological photonic structures evolved by insects provide inspiring examples for the design and fabrication of synthetic photonic crystals. The small scales covering the beetle *Entimus imperialis* are subdivided into irregularly shaped domains that mostly show striking colors, yet some appear colorless. The colors originate from photonic crystals consisting of cuticular material and air, which are geometrically separated by a triply periodic D-surface (diamond). The structure and orientation of the photonic crystals are characterized and it is shown that in colorless domains SiO₂ substitutes the air. The experimental results are incorporated into a precise D-surface structure model used to simulate the photonic band structure. The study shows that the structural parameters in colored domains are optimized for maximum reflectivity by maximizing the stop gap width. The colorless domains provide a biological example of how the optical appearance changes through alteration of the refractive index contrast between the constituting phases.

1. Introduction

In the near future, photonic band gap materials are expected to play the same important role in photonics as semiconductors do in electronics.^[1] Biological photonic crystals, particularly those of insects with their ability to display beautiful colors,^[2,3] provide models to learn the principles used by nature to open up photonic band gaps.^[4–6] Many species of weevils (Coleoptera, Curculionidae) generate strikingly brilliant colors with 3D photonic crystals consisting of cuticular material (chitin and proteins) and air, which are encased in small scales located on their exoskeletons.^[7–12] Based on ultrastructural investigation, the photonic crystals of a number of weevil species have been described and modeled as opal-type structures,^[7] face centered cubic (f.c.c.) inverse opal structures^[8,10,11] and diamond-based structures.^[9] Recently, many biological 3D photonic crystals

have been shown to be bicontinuous cubic structures,^[13,14] whereas those found in scales of weevils correspond to the D-surface (diamond) structure.^[12,13]

Here we investigated scales of the neotropical weevil *Entimus imperialis* to characterize the structure and orientation of the photonic crystals in differently colored domains as well as in previously undescribed colorless domains, where we show that the air phase is substituted by a solid SiO₂ phase. Such modifications result in a change of the refractive index contrast between the constituents that leads to modifications of the photonic stop gap size. This concept is widely used to tune the optical properties of synthetic photonic crystals and is also used to experimentally modify those of natural photonic crystals.^[2,15] A D-surface model based on the

structural parameters obtained from high-resolution scanning electron microscopy (SEM) analysis was used to validate the relationship between orientation and observed colors by calculating the photonic band structure. Simulations reveal that the photonic crystal in the scales of this beetle can possess extremal optical properties. In colored domains, the structural parameters are optimized for opening the largest stop gaps possible for any orientation resulting in maximum reflectivity and thus brilliance, whereas in the same photonic structure the stop gap width is reduced dramatically by decreasing the refractive index contrast between the two phases, which leads to a colorless appearance and transparency of the respective domains.

2. Results and Discussion

2.1. Structural Analysis of the Photonic Crystal

Individual scales from the elytra of *Entimus imperialis* (Figure 1A) are leaf-shaped with slightly convex surfaces, about 100 μm long, 30–60 μm wide, 6 μm thick and show strongly iridescent colors that cover nearly the full visible spectrum (Figure 1B).^[10,12] In contrast to other weevil species,^[8,9] individual colored domains are relatively large and have sharp, defined borders (Figure 1C). Upon close inspection using light microscopy, we observed that certain domains are colorless and appear transparent (Figure 1D).

X. Wu, Prof. D. Raabe, Dr. H.-O. Fabritius
Max-Planck-Institut für Eisenforschung GmbH
Department of Microstructure Physics
and Alloy Design
Max-Planck-Str. 1, 40237 Düsseldorf, Germany
E-mail: h.fabritius@mpie.de



Dr. A. Erbe
Max-Planck-Institut für Eisenforschung GmbH
Department of Interface Chemistry and Surface Engineering
Max-Planck-Str. 1, 40237 Düsseldorf, Germany

DOI: 10.1002/adfm.201203597

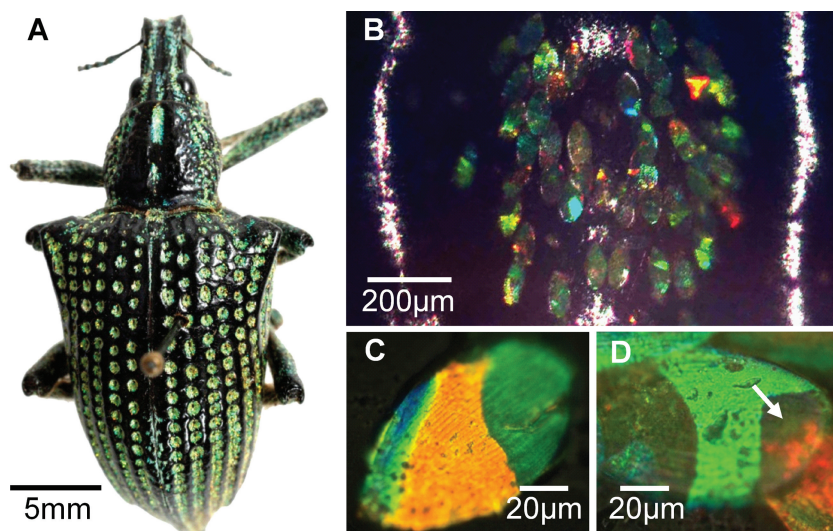


Figure 1. The neotropical weevil *Entimus imperialis* (Coleoptera, Curculionidae). A) Habitus of the investigated specimen. Reproduced with permission.^[30] Copyright 2012, Elsevier. B) Light microscopy image of scales located in a depression on the dorsal surface of the otherwise black elytra. C) Individual scale with three differently colored domains. D) A scale with a colorless domain (arrow) through which the dark orange color of a subjacent scale is visible.

2.1.1. Structure and Orientation of the Photonic Crystal in Colored Domains

In colored scales, exposure of the photonic crystal both parallel and perpendicular to the scale surface using focused ion beam (FIB) milling reveals that fourfold-connected solid struts constitute it. Morphometric measurements on SEM images from all inspected colored domains show that the length of the struts and the angles between them are equal (Figure 2A–D). This arrangement corresponds to the tetrahedral coordination of the fourfold bonded carbon atoms in a diamond lattice and confirms earlier findings in the scales of this and other weevil species.^[9,12] Different observed colors correspond to different orientations of the same photonic crystal in each domain, making every scale act like a photonic polycrystal with a diamond lattice (Figure 2A–D). The structure of this type of photonic crystal is a bicontinuous cubic structure,^[13] where space is divided into two continuous subvolumes, namely, cuticular network and an air phase, separated in this case by a triply periodic intermaterial dividing surface (IMDS)^[16] generating a D-surface structure.^[12,13] Using high resolution scanning electron micrographs of all exposed domains, we morphometrically derived the parameters necessary to calculate a D-surface model that exactly reproduces the biological photonic structure. We measured the distances between neighboring ramification points in the respective $\langle 110 \rangle$ direction in all exposed domains and used the average value of $288 (\pm 8)$ nm to determine the lattice constant, which is $407 (\pm 11)$ nm. The thickness of the struts is similar in all investigated domains and amounts to an average of $98 (\pm 7)$ nm. The equal lattice constant and thickness of the struts in all domains implies that the volume fraction of cuticular material is uniform over all scales. We quantified this volume fraction by measuring the diameter of the holes and the thickness of the neck of the struts in yellow domains (Figure 2A) and determined the ratio to be $1.61 (\pm 0.07)$. Subsequently, the

D-surface model was adapted by fine tuning the parameter t (for details see Experimental Section) until the ratio between hole diameter and strut thickness equaled the experimentally determined value. The obtained t is $0.36 (\pm 0.03)$, resulting in volume fractions of 35% cuticular material and 65% air ($\pm 1.5\%$), respectively. The orientation of the photonic crystal in differently colored domains was determined by cutting visualizations of the D-surface model along different crystallographic lattice planes (insets in Figure 2A–D) to exactly fit the structures observed in situ. Upon identical visual appearance of structure and model, the Miller index of the exposed lattice plane corresponds to the orientation of the photonic crystal in each sample with respect to the scale surface. The corresponding normal directions of the lattice planes oriented parallel to the scale surface (Figure 2A–D) are close to the $\langle 111 \rangle$ direction in yellow domains, the $\langle 100 \rangle$ direction in green and light blue domains and the $\langle 110 \rangle$ direction in dark blue domains.

2.1.2. Structure and Orientation of the Photonic Crystal in Colorless Domains

Colorless, transparent scales have been observed before in the weevil *Pachyrhynchus argus*^[7] and have been explained by the absence of an inner opal-type photonic crystal as found in colored scales. Therefore, it was surprising that removal of the shell on colorless domains using FIB exposed a solid core showing clearly distinguished periodic patterns of light and dark contrasted features (Figure 2E,F) whose arrangement and dimensions resembled the section profiles of the solid phase in exposed surfaces of the photonic crystal in colored domains (Figure 2). By adjusting visualizations of the D-surface model for colored domains cut along different crystallographic lattice planes, it was possible to match the section profile of the solid phase to the pattern of the dark contrasted features observed in colorless domains. When they match, the complementary light contrasted areas resemble the section profile of the air phase (Figure 2E,F). This similarity indicates that colorless and colored domains contain structurally similar 3D photonic crystals, which implies that the air in colorless domains is substituted by a solid phase.

2.1.3. Composition of the Second Solid Phase in Colorless Domains

Comparison of qualitative energy-dispersive X-ray (EDX) spectra recorded on exposed colorless and colored domains of the same scale show an almost equal carbon to oxygen ratio and an additional, strong silicon peak in colorless domains (Figure 3A). Under the assumption that the composition of the cuticular phase is the same in both types of domains, the elevated silicon and oxygen signals should originate from the solid second phase present in the colorless domains. This is supported by the high electron optical contrast between the two phases observed in the colorless domain, which should not

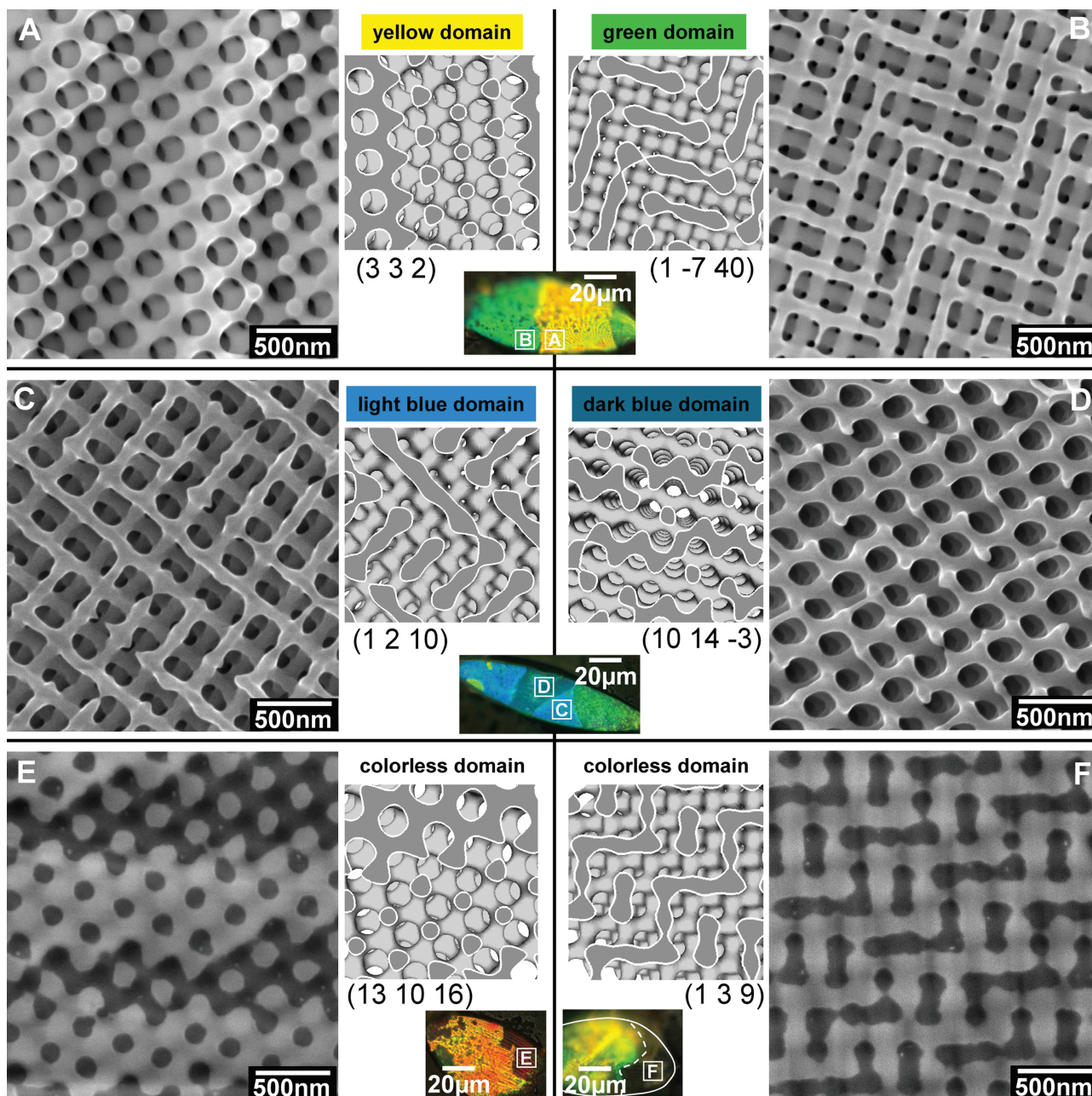


Figure 2. Microstructure of the photonic crystal in colored and colorless domains. The electron microscopy images show the photonic crystal exposed parallel to the scale surface. The grayscale inserts show corresponding visualizations of the D-surface model. The numbers are Miller indices of the exposed lattice planes for A) yellow (3 3 2); B) green (1 -7 40); C) light blue (1 2 10); D) dark blue (10 14 -3), and E,F) two colorless domains; E) (13 10 16) and F) (1 3 9). The inset light microscopy images show the exact probed locations on the respective scales.

appear due to the absence of topological contrast of the samples resulting from FIB preparation (Figure 2E,F). However, since we used an in-lens detector, which can also detect back scattered electrons that generate characteristic atomic number contrast, the silicon rich phase appears light and the carbon rich cuticular network dark contrasted.

Transmission Fourier transform infrared (FTIR) spectra (Figure 3B) obtained from a scale with a colored domain and a colorless domain (Figure 3C, right) reveal the presence of two strong peaks at 1020 and 1091 cm^{-1} in the colorless domain,

which are typical for Si-O stretching modes from SiO_4 tetrahedra^[17–20] and are absent in the colored domain. An integration of the absorbance between 950 and 1150 cm^{-1} in spectra from different parts of the scale (Figure 3C, left) shows that the distribution of the Si-O modes (purple region in Figure 3C, left) is confined to the colorless domain (Figure 3C, right). Two peaks at 1261 cm^{-1} and 2964 cm^{-1} are of significantly higher intensity in the colorless domain compared to the colored domain. The latter can be attributed to a C-H stretching mode.^[21] For the former, several possibilities exist,^[21] though

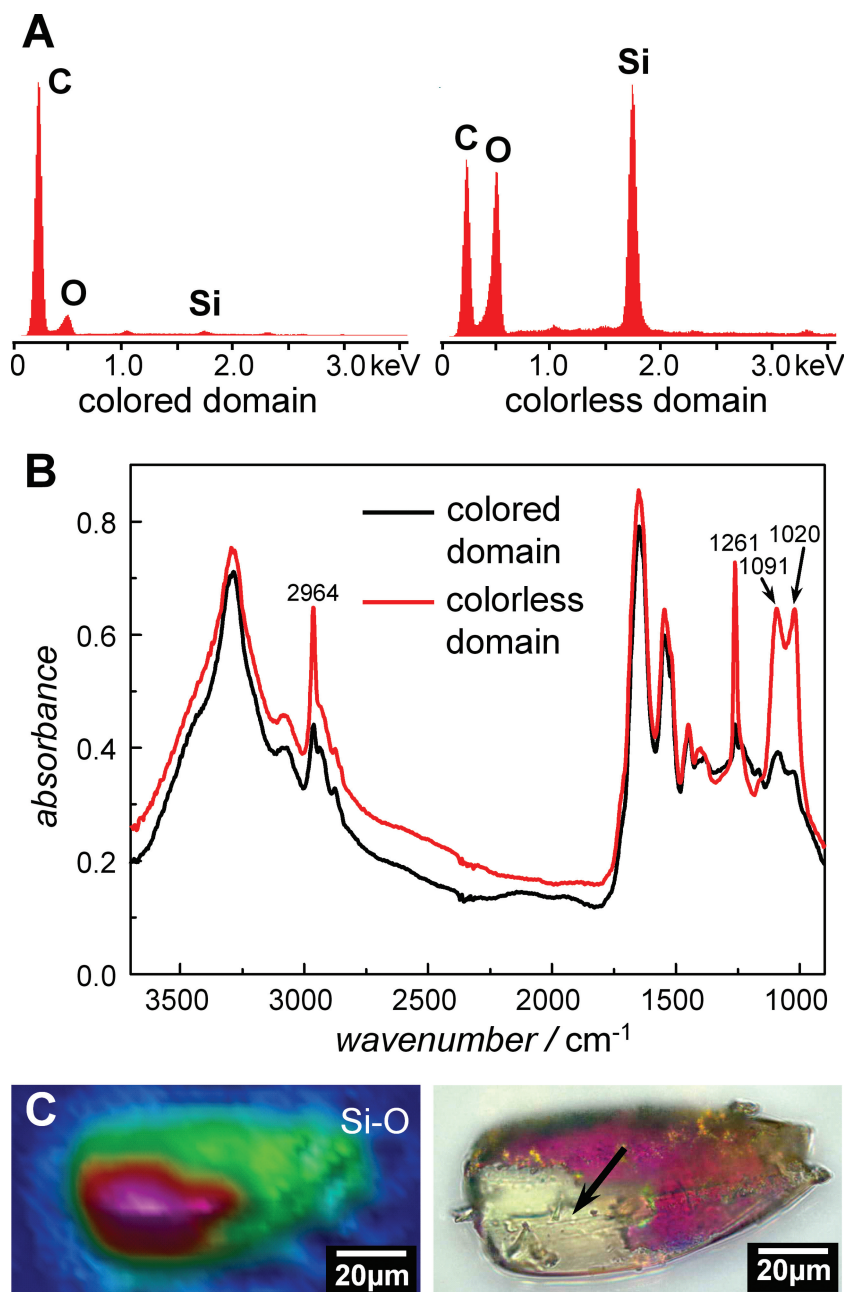


Figure 3. Chemical composition of scales with transparent domains. A) Qualitative elemental distribution in a colored (left) and a colorless (right) domain of the same scale. The EDX spectra show that the colorless domain is rich in Si and O. B) Transmission FTIR spectra of the colorless (red line) and colored (black line) domain. C) Left: Spatial distribution of the integrated absorbance from transmitted light of the Si-O stretching mode spectral region (blue: weak integral absorbance, purple: strong integral absorbance). Right: Light microscopy image of the analyzed scale (arrow: colorless domain).

no Si-O related modes have been described in minerals in this region to our knowledge.^[19] The peaks at 1650 cm⁻¹ (protein amide I mode^[22]) and 1545 cm⁻¹ (protein amide II mode^[22]) are of equal intensity and shape in both domains, which implies equal protein content and structure. Together with the structural resemblance, this supports the assumption that the cuticular network is similar in both domains. Therefore, the additional CH peak indicates the presence of additional organic

material besides silicon oxide species in the colorless domain. Although the existence of silicon in the scale of this weevil seems to be surprising, together with silicon, many inorganic elements can be found in the cuticle of insects.^[23,24] The high abundance of silicon and oxygen elements in the second phase of the colorless domains indicates the existence of a type of silicon oxide. No significant amounts of other elements typically present in silicate minerals, such as Na, K, Ca or Al have been found. In addition, the IR spectra show the presence of Si-O modes typical for the most abundant four-fold coordinated silicon in SiO₂.^[17,18] Other forms of SiO₂ exist, but are extremely rare.^[25]

In the light of earlier studies of the weevil *E. imperialis*^[10,12] and due to the lack of further specimens to investigate, we can at present not definitely conclude that the SiO₂ present in colorless scales is originating from the beetles themselves, since it could also be the result of contamination processes that occurred in vivo or post mortem during storage in museum collections. Concerning post mortem contamination, we traced potential scenarios, e.g., conservation method, preservation agents etc. to the best of our knowledge without being able to find evidence for artificial SiO₂ sources. However, the fact that colorless scales were found in the species *P. argus*^[7] as well indicates that they are truly synthesized by the animals themselves. Furthermore, the FTIR spectra of the SiO₂ modes observed here closely resemble those observed in biogenic silica and show substantial differences to man-made SiO₂ where the peaks at 1090 and 1020 cm⁻¹ are usually not of equal intensity.^[26] Since these beetles are phytophagous and many plants contain SiO₂, their diet might be a possible source for the mineral. However, a physiological mechanism for the incorporation of SiO₂ into the photonic crystals inside the scales of *E. imperialis* has not been described yet. If SiO₂ is actively metabolized by the beetles, one would have to bring up the question what purpose this could serve and whether it is incorporated during the development or after the full differentiation of the scales. At the current state of our knowledge, we can only speculate about the biological role of such an adaptation, but this is certainly a very interesting topic for further investigation. Regardless of the provenience of SiO₂ in the colorless domains of the scales and its potential functions, the principle of replacing one phase of a 3D photonic crystal by another one with different refractive index is a highly interesting concept from a materials science point of view, since it is a natural example for photonic crystals with tunable optical properties.

2.2. Correlation of Structure and Composition with the Optical Properties of the Photonic Crystals

To validate our structural analysis of the photonic crystal in colored and colorless domains of scales and compare their optical properties, we used the adjusted D-surface structure model to calculate the photonic band structure.^[27] The refractive

index of the cuticular network^[28] was assumed to be 1.56. Since it is known that the refractive index of most of the polymorphs of silica^[29] ranges from 1.4 to 1.6, we used 1.5 for the SiO₂ phase.

The resulting photonic band diagram (Figure 4A) shows partial band gaps in different directions. For colored domains, the wavelength range of stop gaps calculated for the lattice constant of 407 nm in this beetle are 527–603 nm for Γ -L $\langle 111 \rangle$

(yellow domain, Figure 2A), 476–513 nm for Γ -X $\langle 100 \rangle$ (green and light blue domains, Figure 2B,C) and 453–492 nm for Γ -K $\langle 110 \rangle$ (dark blue domain, Figure 2D). The observed colors in differently oriented domains and the wavelength ranges of the stop gaps in the corresponding directions are in good agreement (Figure 4A). These results are in accordance with those of an earlier study, where the authors visualized the angular spectral response of single domains in *E. imperialis* scales using imaging scatterometry.^[12] By varying the volume fraction of the cuticular material from about 8% to 92% (corresponding to t varying from 1 to -1), the stop gaps calculated for all investigated colored domains obtain their widest frequency ranges when the volume fraction is close to 35%, the value we determined for the beetle (Figure 4B). Optically, a stop gap covering a wider frequency range not only means more hues included, but also implies that a larger fraction of the incident white light is reflected. Thus, the scales show a stronger reflection and appear more brilliant.

In contrast, the combination of the SiO₂ phase and the cuticular phase in colorless domains shows only very narrow photonic stop gaps due to the very small refractive index contrast between them (Figure 4A). These narrow gaps only allow a very small fraction of the incident light to be reflected while the rest is transmitting through the scale. This weak reflection is sensitive to scattering. As a result, the domain consisting of these two phases appears transparent and dull to the eye.

3. Conclusions

Thus, although the basic structure of the cuticular phase is uniform in all elytral scales of the weevil *E. imperialis*, they can have extremal optical properties. In colored domains, evolutionary pressures that have favored the development of brilliant colors have led to optimal volume fractions for opening the broadest stop gap possible independent of orientation, whereas in colorless domains the width of the stop gaps is dramatically reduced by substitution of the air phase with a SiO₂ phase whose refractive

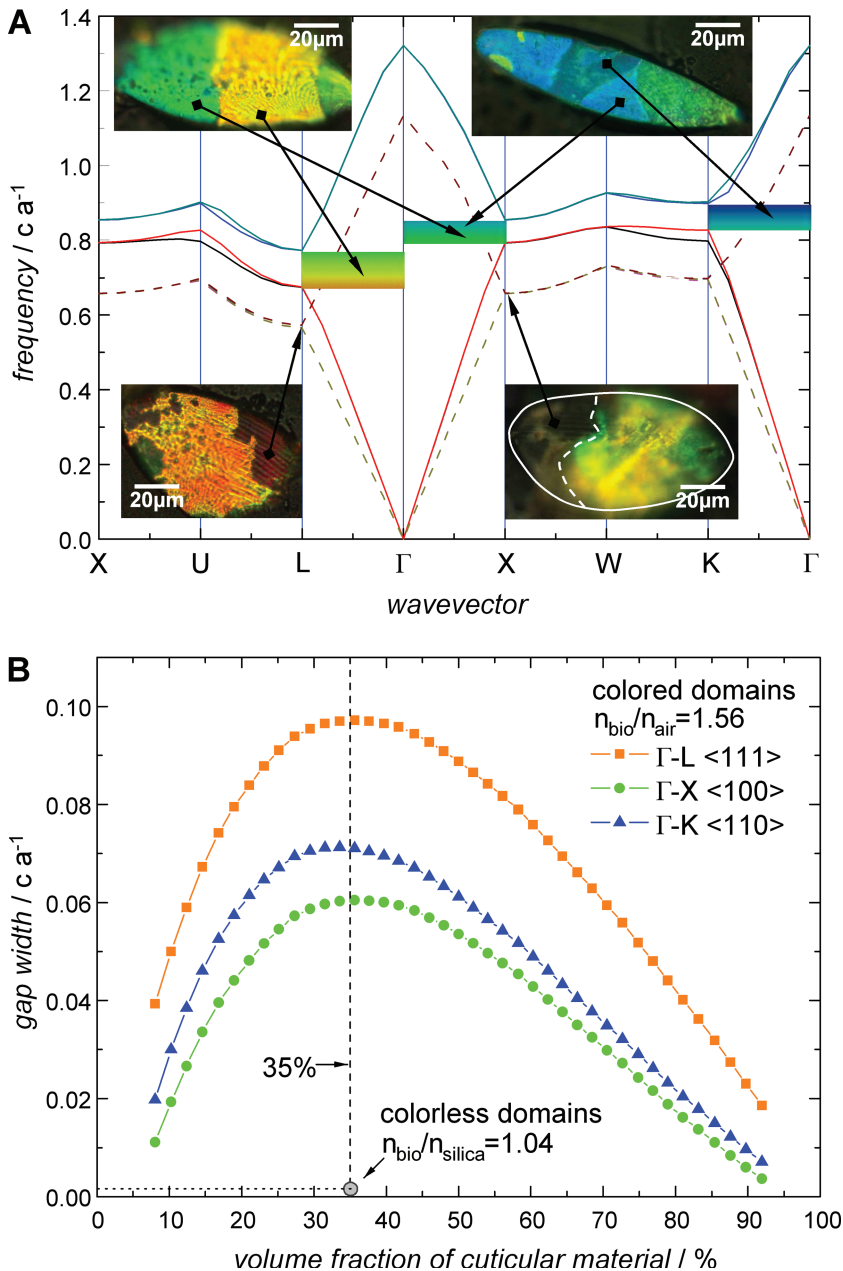


Figure 4. Optical properties of the photonic crystal in colored and colorless domains. A) Photonic band diagram for colored and colorless domains calculated using the parameterized D-surface model. The probed locations (light microscopy images) and the color range of the stop gaps (arrows) for the corresponding directions are shown as inserts. B) Stop gap width as a function of varying volume fractions of cuticular material ($t \in [1, -1]$). For colored domains with relatively high refractive index contrast, the stop gaps (orange: $\langle 111 \rangle$; green: $\langle 100 \rangle$ and blue curve: $\langle 110 \rangle$) obtain their widest frequency ranges at a volume fraction close to 35% (dashed line) as observed in the beetle. For colorless domains with low refractive index contrast, the stop gaps are very narrow (circle).

index is close to that of the cuticular material. Modification of the photonic stop gap width, and thus the optical appearance, by replacing the air phase of a 3D photonic crystal with a second solid phase was observed for the first time in a beetle. The intriguing structural characteristics of the scales of *E. imperialis* make them ideal biotemplates for the fabrication of tunable photonic crystals operating in the visible frequency range.^[30]

4. Experimental Section

E. imperialis specimens used for this study were obtained from the entomological collections of the Staatliches Museum für Naturkunde Stuttgart courtesy of Dr. Joachim Holstein, who also helped in determining the species.

Structural Characterization using FIB and SEM: The scales were scraped from the surface of the cuticle with a needle. The photonic structure within the scales was exposed by milling in a focused ion beam (FIB) microscope combined with scanning electron microscopy (SEM) (Zeiss Gemini 1540 XB). For FIB preparation, scales were glued to the surface of self-adhesive carbon pads mounted on cylindrical plastic holders. In order to study the 3D architecture of the photonic structure and minimize milling artifacts we first removed the shell at the margins of scales perpendicular to their surface followed by milling in grazing incidence parallel to the surface. All samples were inspected using light optical microscopy (LOM, Leica DM 4000M) in bright field mode and SEM using an in-lens detector at low acceleration voltage (5 keV) to minimize beam damage. For SEM, the plastic holders were mounted to standard aluminum holders and rotary shadowed with 2 nm platinum using a precision etching coating system (Model 682, Gatan Inc.).

Analysis of Chemical Composition: Qualitative energy dispersive X-ray (EDX) spectra of the scales were recorded using an EDAX system (PV7716/08 ME) attached to the SEM. For measurement of Fourier transform infrared spectra (FTIR, Bruker Hyperion 3000 IR microscope on Vertex 70v spectrometer), individual scales were placed on a double sided polished piece of germanium measuring 2 cm × 4 cm. Spectral images were measured in transmission geometry on the microscope's 64 × 64 pixel focal plane array detector, and referenced against a region of the germanium piece without scales.

Reconstruction of D-Surface Model: The photonic structure was reconstructed by a D-surface structure model,^[13,16,31] which can be approximated by a constant mean curvature surface modeled by a level surface:

$$f(x, y, z) = \cos Z \sin(X + Y) + \sin Z \cos(X - Y) = t \quad (1)$$

where $X = 2\pi x$, $Y = 2\pi y$ and $Z = 2\pi z$. (x, y, z) are the coordinates of the crystal structure. The parameter t determines the fractions of the two continuous volumes divided by the D-surface. For this study, we assign the volume defined by $f(x, y, z) > t$ to represent the solid cuticular material and the complementary volume as the air phase. The model was adapted to the photonic crystal of *E. imperialis* by adjusting t according to the determined ratio between the diameter of the holes and the thickness of the neck of the struts from SEM images (Figure 2). The resulting model was visualized (Figure 2, insets) using the open source software K3DSurf.^[32]

Photonic Band Gap Calculation: Based on the D-surface structure model, the photonic band structure was calculated by solving Maxwell's equations for eigenmodes in the frequency-domain using the MIT Photonic-Bands (MPB) package.^[27] The refractive index of the cuticular network was assumed to be 1.56,^[28] the one for SiO₂ phase is 1.5^[29] and the one for air is 1.00. The lattice constants of the photonic crystal in different domains were determined by measuring the dimensions of the solid photonic crystal network on the recorded SEM images (Figure 2).

Acknowledgements

The authors wish to thank Dr. Joachim Holstein (Staatliches Museum für Naturkunde Stuttgart) for providing the beetle specimens,

Petra Ebbinghaus (Department of Interface Chemistry and Surface Engineering, MPIE) for performing the IR experiments, and the Max-Planck-Society for financial support.

Received: December 5, 2012

Revised: January 28, 2013

Published online: March 12, 2013

- [1] J. D. Joannopoulos, S. G. Johnson, J. N. Winn, R. D. Meade, *Photonic Crystals: Molding the Flow of Light*, 2nd ed. Princeton University Press, Princeton **2008**.
- [2] S. Kinoshita, *Structural Colors in the Realm of Nature*, World Scientific Publishing, Singapore **2008**.
- [3] A. E. Seago, B. Parrish, J.-P. Vigneron, T. D. Schultz, *J. R. Soc. Interface* **2009**, 6, S165.
- [4] P. Vukusic, J. R. Sambles, *Nature* **2003**, 424, 852.
- [5] A. R. Parker, *J. R. Soc. Interface* **2005**, 2, 1.
- [6] S. Kinoshita, S. Yoshioka, *Chem. Phys. Chem.* **2005**, 6, 1442.
- [7] A. R. Parker, V. L. Welch, D. Driver, N. Martini, *Nature* **2003**, 426, 786.
- [8] V. Welch, V. Lousse, O. Deparis, A. Parker, J. P. Vigneron, *Phys. Rev. E* **2007**, 75, 041919.
- [9] J. W. Galusha, L. R. Richey, J. S. Gardner, J. N. Cha, M. H. Bartl, *Phys. Rev. E* **2008**, 77, 050904.
- [10] O. Deparis, J. P. Vigneron, *Mat. Sci. Eng. B* **2010**, 169, 12.
- [11] C. Pouya, D. G. Stavenga, P. Vukusic, *Opt. Express* **2011**, 19, 11355.
- [12] B. D. Wilts, K. Michielsen, H. D. Raedt, D. G. Stavenga, *J. R. Soc. Interface* **2012**, 9, 1609.
- [13] K. Michielsen, D. G. Stavenga, *J. R. Soc. Interface* **2008**, 5, 85.
- [14] V. Saranathan, C. O. Osuji, S. G. J. Mochrie, H. Noh, S. Narayanan, A. Sandy, E. R. Dufresne, O. R. Prum, *Proc. Natl. Acad. Sci. USA* **2010**, 107, 11676.
- [15] S. Kinoshita, S. Yoshioka, J. Miyazaki, *Rep. Prog. Phys.* **2008**, 71, 076401.
- [16] H. G. von Schnering, R. Nesper, *Z. Phys. B Condens. Matter* **1991**, 83, 407.
- [17] J. Etchepare, M. Merian, L. Smetankine, *J. Chem. Phys.* **1974**, 60, 1873.
- [18] J. Etchepare, M. Merian, P. Kaplan, *J. Chem. Phys.* **1978**, 68, 1531.
- [19] V. C. Farmer, *The Infrared Spectra of Minerals*, Mineralogical Society Monograph 4, Mineralogical Society, London **1974**.
- [20] A. M. Efimov, *Optical Constants of Inorganic Glasses*, CRC Press, Boca Raton **1995**.
- [21] R. A. Nyquist, *Interpreting Infrared, Raman, and Nuclear Magnetic Resonance Spectra*, Vol. 1., Academic Press, Waltham **2001**.
- [22] E. Goormaghtigh, V. Cabiaux, J. M. Ruyschaert, in *Subcellular Biochemistry*, Vol. 23 (Ed: G. B. Ralston, H. J. Hilderson), Plenum Press, New York **1994**, pp. 363.
- [23] A. G. Richards, *J. Histochem. Cytochem.* **1956**, 4, 140.
- [24] M. Rockstein, *The Physiology of Insecta* Vol. VI., Univ. of California, Academic Press, New York, London **1974**.
- [25] R. J. P. Lyon, *Nature* **1962**, 195, 266.
- [26] F. Sandford, *Microsc. Res. Tech.* **2003**, 62, 336.
- [27] S. G. Johnson, J. D. Joannopoulos, *Opt. Express* **2001**, 8, 173.
- [28] P. Vukusic, J. R. Sambles, C. R. Lawrence, R. J. Wootton, *Proc. R. Soc. London B. Biol.* **1999**, 266, 1403.
- [29] B. J. Skinner, D. E. Appleman, *Am. Mineral.* **1963**, 48, 854.
- [30] D. Van Opdenbosch, M. Johannes, X. Wu, H. Fabritius, C. Zollfrank, *Photonics Nanostruct. Fund. Appl.* **2012**, 10, 516.
- [31] M. Wohlgemuth, N. Yfa, J. Hoffman, E. L. Thomas, *Macromolecules* **2001**, 34, 6083.
- [32] A. Taha, K3DSurf: 3d surface generator. URL: <http://k3dsurf.sourceforge.net/>, **2012** (accessed August 2012).